COBEM 2021 26th International Congress of Mechanical Engineering
November 22-26, 2021, Virtual Congress, Brazil

COB-2021-0257
STEREO-PIV MEASUREMENT OF TURBULENT FLOW IN A SQUARE DUCT

Leonardo Soares Fernandes
Pontifícia Universidade Católica do Rio de Janeiro, Department of Mechanical Engineering, 22451-900, Rio de Janeiro, RJ, Brazil
leonardofernandes@puc-rio.br

Luis Fernando Alzuguir Azevedo
Pontifícia Universidade Católica do Rio de Janeiro, Department of Mechanical Engineering, 22451-900, Rio de Janeiro, RJ, Brazil
lfaa@puc-rio.br

Abstract. *Turbulent flows in ducts with a square cross section are found in many engineering applications, such as ventilation systems and combustion engines. Moreover, its relatively simple geometry is useful to study the effect of the less intense secondary flows on the overall flow structure, and other quantities of interest, such as pressure drop and wall shear stresses. The present work studies first and second-order velocity statistics inside a water channel with a square cross-section of 40x40 mm^2. The experimental design allows for measurements of pressure drop and three-component velocity vector fields, using the Stereoscopic Particle Image Velocimetry (SPIV) technique. Preliminary results show secondary motions at the duct corners, which influence the mean streamwise velocity field. This behavior was already reported in the literature, but detailed data was based on direct numerical simulations (DNS). The mean velocity fields and Reynolds stress tensors results obtained can be used both to serve as a base case for studies with drag-reducing agents as well as to improve the performance of turbulence models using Machine Learning based procedures. Both these studies are the next phase of this work.*

Keywords: *Stereo-PIV, Turbulence, Reynolds stress, Square duct flow*

1. INTRODUCTION

Turbulent flows in square duct channels are commonly found in a wide range of engineering applications. Typical technical examples are combustion engines, sewer systems and refrigeration systems. In addition, its simple geometry facilitates the study of three-dimensional flow features presented in wall-bounded turbulent flows. One of these interesting characteristics of turbulent flow in square ducts is the development of secondary flows, and its influence on the mean streamwise flow. Despite the fact that these motions have been reported in the literature, its influence on the overall flow characteristics remain a topic of current research interest (Vinuesa et al., 2014).

In square channels, the secondary flow consists of 4 pairs of streamwise counter-rotating vortices, located at the channel corners. This behavior was reported by many authors in the literature, either based on Direct Numerical Simulations (DNS) (Uhlmann et al., 2007; Vinuesa et al., 2014) or measurements with probes (Gessner and Jones, 1965; Gessner, 1973). Despite the fact that secondary flows present typically only 2-3% of the bulk streamwise velocity magnitude (Huser and Biringen, 1993), it modifies the streamwise averaged velocity profile. The vortices convect momentum from the wall to regions along the corner bisector, accelerating the flow close to the corners and decreasing the streamwise velocity along the walls. Despite the large number of works in the literature presenting velocity fields and turbulent structures in a square duct, the majority of them are based on DNS data, what restricts their investigations to relatively low Reynolds numbers, due to computational capacity limitations. One goal of the present study is to provide detailed data in flows with higher Reynolds numbers. This was achieved by employing the Stereoscopic PIV technique (SPIV), capable of measuring the three-components of the velocity vector in a cross section plane. The data obtained will also serve as a base case to, in the future, study the effects of drag-reducing polymers on the flow structures.

Another important aspect of the present study is the fact that in industrial applications of the flows mentioned above, the most common approach is to model turbulence using Reynolds-averaged Navier-Stokes (RANS) models, due to its relatively lower computational cost. However, according to Launder (1990) and Vinuesa et al. (2014), traditional RANS models, which are based on Boussinesq´s approximation, fail to predict secondary flow effects. This happens due to the simplified anisotropic model used to represent the Reynolds stress tensor. In this context, more elaborate constitutive models of the Reynolds stress tensor are necessary, which better account for anisotropic effects, such as the one presented by Spalart (2000). Not only the author was capable of predicting secondary flows, but his results were in better agreement with experimental data for a square channel. This shows how RANS models can be improved by a deeper understanding of the physics governing the flow. This shows another relevant use of the data measured in this work, which can also be extended to the flow with drag-reducing polymers. Also, recently machine learning techniques have been used to train

and improve the prediction capabilities of RANS models (Cruz et al., 2019). These studies normally make use of DNS databases as an input to the algorithms. As already mentioned, these data are obtained for limited values of Reynolds number. An experimental database obtained at higher Reynolds numbers, such as the one provided by the present work, could be valuable information for these machine learning techniques initiatives.

This work is part of an ongoing research on turbulence, at the Laboratory of Fluid Engineering, at PUC-Rio. The results presented here consist of the validation of the measurements by comparing it with the DNS from Pinelli et al. (2010).

2. EXPERIMENT

The Stereoscopic PIV technique employed in the present work provided three-component velocity fields in a transversal plane crossing the square duct. The plexiglass test section utilized was 4-m long, with a 40x40 mm2 flow cross section (Figure 1). Pressure taps in the form of 1-mm holes were installed along the test section, equally spaced of 250 mm. Water was used as working fluid, and it was driven into the test section by a progressive cavity pump, controlled by a frequency inverter. Plenum chambers were positioned both at the outlet and at the inlet of the test section, in order to attenuate oscillations caused by the pump and by geometry changes of the returning pipe. A 1x1mm screen was installed just downstream of the inlet plenum box. It had the dual function of destroying large-scale vortices generated in the inlet pipe bends, and of accelerating the development of the turbulent flow.

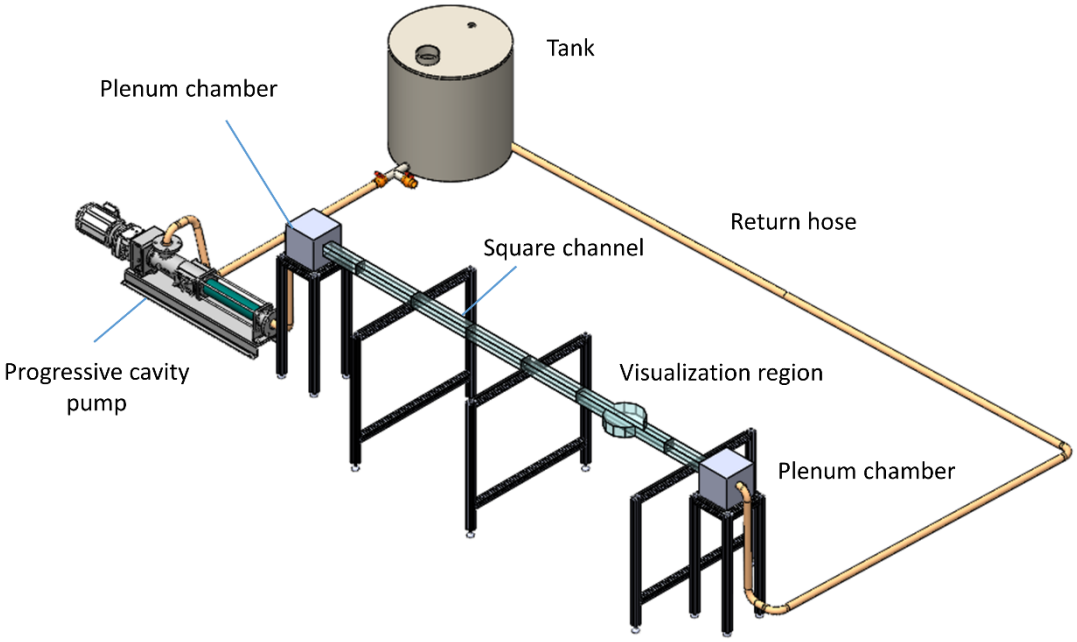

Figure 1 - Schematic view of the test section.

The measurement section was composed by two CMOS Phanton M340 cameras (2560x1600 pixels) equipped with expansion rings and 105-mm Micro Nikon-Nikkor lenses with f#8 apertures, mounted on Scheimpflug adaptors. A 610036 TSI synchronizer was responsible for controlling camera acquisition and the laser pulses, provided by a Nd:YAG dual cavity Evergreen laser (200mJ/pulse at 15Hz). The cameras were positioned at opposite sides of the laser light sheet, and at the same side of a visualization box, with a 90º angle between them, as indicated in Figure 2.

The visualization box consisted of two prisms, mounted symmetrically around the square channel and filled with water. This system not only attenuated optical distortions, but also allowed multiple optical accesses to the measurement section. Specifically, in the measurement region, the upper part of the square channel could be removed, providing easy and quick access to the square channel. This was specially designed so that a calibration target could be placed inside of the channel.

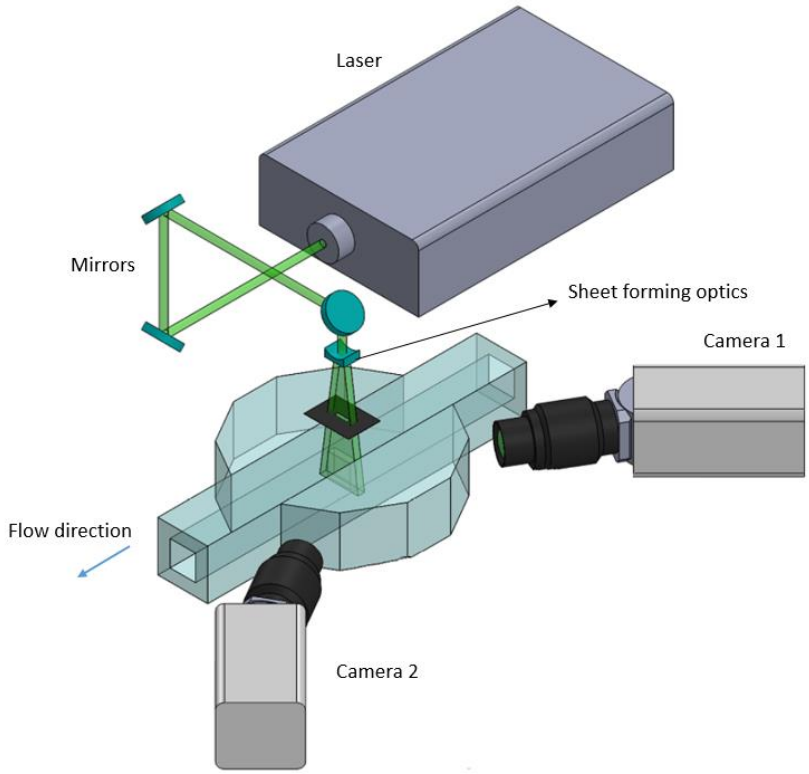

Figure 2 – Schematic view of the measurement region.

When performing Stereoscopic PIV, the cameras must be calibrated. The common approach is to use a calibration target, which is placed inside the measurement region. In this work, the calibration target consisted of a matrix of equally-spaced points, printed in a transparent sheet, as shown in figure 3a. The target was connected to a support base which was fixed to a translational stage, controlled by a Mitutoyo Micrometer (figure 3b). This simple assembly allowed the translation of the target along the measurement region. Images of the target were acquired at five equally-spaced planes along the laser sheet thickness, spaced by 0.25mm. During the calibration procedure, two lamps positioned symmetrically to the cameras, at the secondary prism were responsible to provide back illumination of the transparent target utilized.

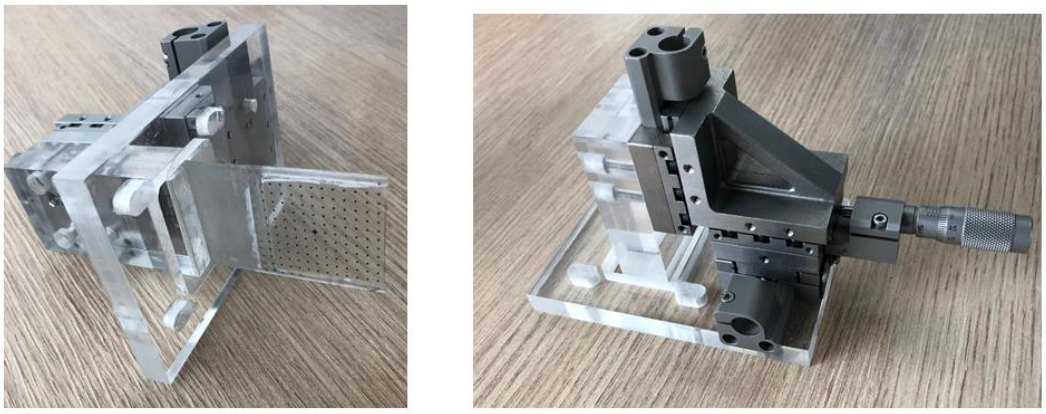

Figure 3 - (a) Detail of the transparent target used in the SPIV calibration and connected to the (b)Translational stage used to move the calibration target inside the square channel.

The pressure holes positioned upstream and downstream of the measurement region were connected to an Omega capacitive pressure transducer, to measure the pressure gradient along the square channel. The voltage output of the pressure transducer was plugged into a National Instrument Data Acquisition Board. The averaged pressure gradient was then calculated using a routine developed in the software Labview.

3. EXPERIMENTAL PROCEDURE

In order to validate the experiment test section, measurements were performed with a Reynolds number based on the hydraulic diameter of the square channel of approximately 7000, to match the DNS results from Pinelli et al. (2010).

A total of 9200 image pairs were acquired, for each camera, at a frequency of 15 Hz. This number of independent samples were enough to guarantee well converged fields for all components of the Reynolds stress tensor, as can be seen in Figure 4. The y-axis presents the normalized error between consecutive 200 samples. It is clear that after approximately 6500 samples, the maximum error no longer decay, but remains in a plateau, due to experimental uncertainties.

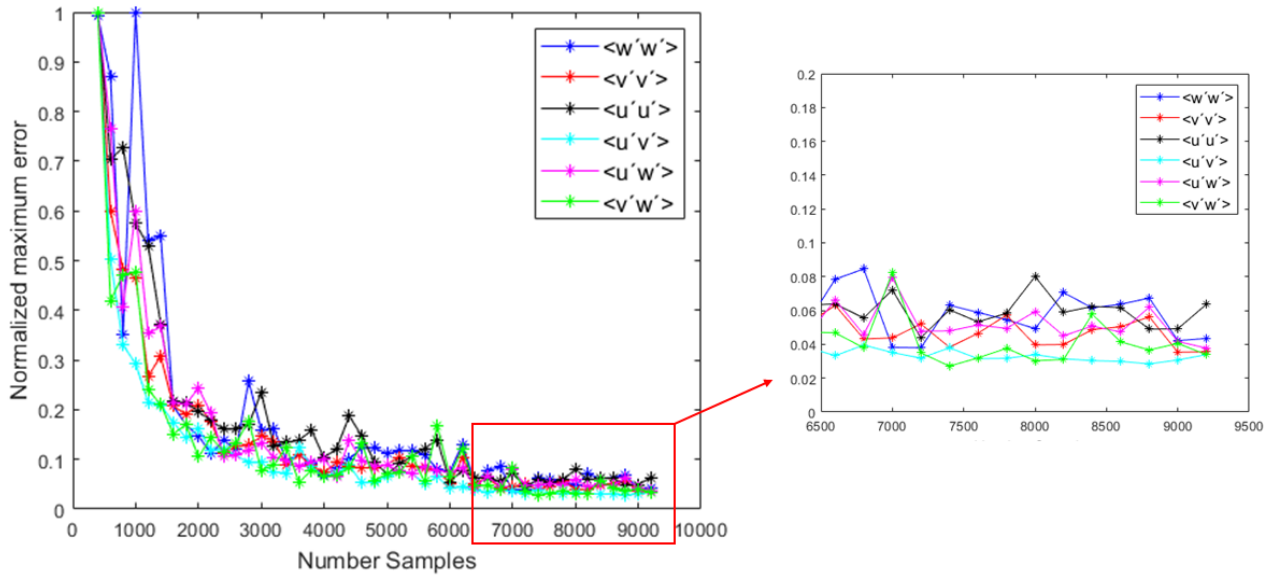

Figure 4 – Normalized error on the different components of the Reynolds stress tensor, with the number of independent samples used to calculated de tensor components.

For each image, laser reflections at the channel walls were minimized by subtracting the intensity background, calculated from the moving time-averaged window of 800 images in a time series. The images were then dewarped by a second-order polynomial and cross-correlation was performed using a multi-pass interrogation scheme with a final cross-correlation window of 32 x 32 pixels and 50% of overlap. The three-component vectors were then reconstructed, leading to 9200 independent vector fields. The moving time-average calculation was performed by a routine developed on Matlab, while all other operations were performed using the software Insight 4G, by TSI. The mean velocity field was calculated by time-averaging the 9200 velocity fields.

Measuring the secondary flows is a difficult task, since the magnitude of in-plane velocity fields are approximately only 2-3% of the mean streamwise velocity component. Since the Stereoscopic-PIV technique measures the three-components of the velocity vector using the laser sheet as a reference, even small miss alignments between the laser plane and the plane perpendicular to the channel cross-section would generate a contamination of the in-plane measurements by a decomposed part of the streamwise component. In fact, as a rule of thumb, even small miss alignments of the order of 1º would generate a projection of the order of sin(1º) of the steamwise velocity on the in-plane measurements, which is 1.75% of its magnitude. This projection is of the same order of magnitude as the in-plane components. This problem was by-passed by using the symmetry of the square channel. A positive decomposition in one quadrant would mean a negative decomposition into another, so by averaging all quadrants (or depending on the quantity, all octants) of the square channel, one can by-pass this issue. This methodology was applied to both the velocity and Reynolds stress components, using the quadrant or octant symmetry, when possible. The results were significantly improved by doing so. It is important, however, to state that this methodology artificially introduces a symmetry to the flow, which is not necessarily true due to possible imperfections in the test section geometry.

During the experiments, the pressure gradient was measured, yielding a value of 11.6 Pa/m, consistent with the theoretical value based on the hydraulic diameter, of 12.3 Pa/m. The error of around 6% corresponds, at this Reynolds number, to less than 3 Pa of the measured pressure difference, which is within the pressure transducer uncertainty.

4. RESULTS

4.1 MEAN VELOCITY MEASUREMENTS

Given the averaged procedure using the symmetry of the square duct described in section 3, all quantities will be presented here only for the third quadrant.

Figure 5 presents isocontours of the streamwise component (W) of the velocity vector divided by the bulk velocity, while vectors represent in-plane components (U and V). The coordinates are made dimensionless by the half-length of the hydraulic diameter (h). As one can see, the pair o counter-rotating vortex was well captured, with the center of each vortex located approximately at the coordinates -0.55 and -0.8. It is clear the effect of those vortices on the transport of fluids with lower momentum from regions close to the wall to the center of the channel (X/h and Y/h > -0.6), and with higher momentum, from the center of the channel all along the corner bisector (X/h and Y/h < -0.6).

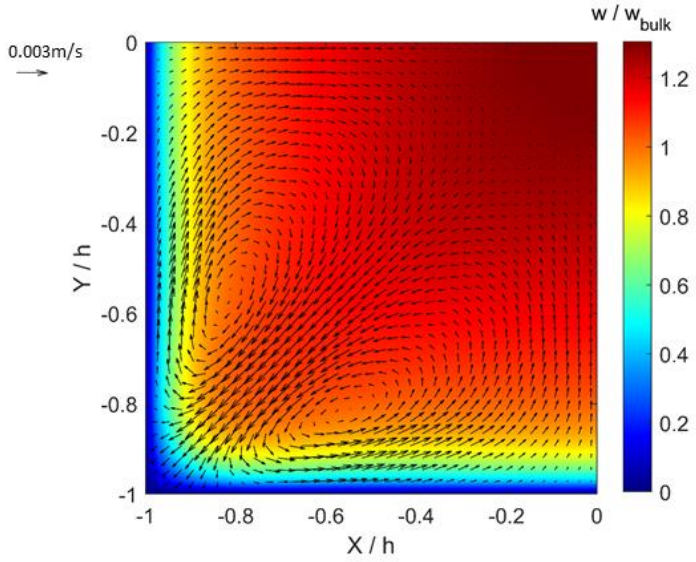

Figure 4 – Streamwise and in-plane components of the velocity vector displayed in the lower left quadrant of the square duct cross section

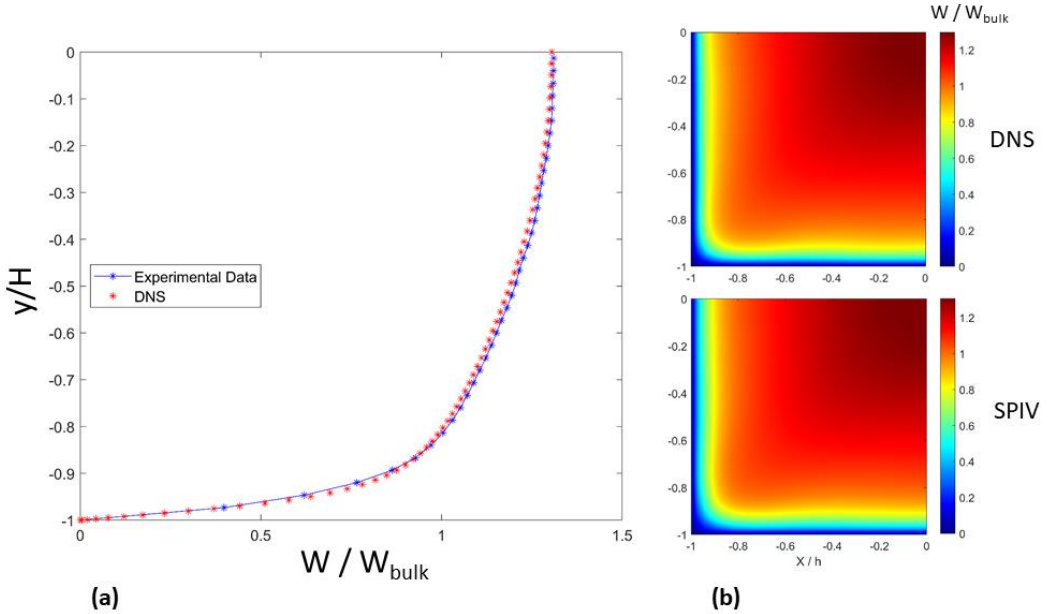

Figure 5 – Comparison between measured SPIV streamwise velocity with data obtainted from the DNS simulations of Pinelli et al. (2010) for (a) velocity profiles and (b) isocontourns.

A comparison of the streamwise velocity profile obtainted from the measurements with SPIV and the DNS data from Pinelli et al. (2010) along the channel center-line X /H = 0 is presented in figure 5(a), while a comparison of the streamwise isocontours of the velocity vector in the quadrant is presented in figure 5(b). For both cases, an excellent agreement can be observed.

Since the pressure gradient was measured, the mean shear stress could be calculated, what allowed for the calculation of the friction velocity ($u_\tau = \sqrt{\frac{\tau_w}{\rho}}$). The experimental velocity profile can, therefore, be plotted in wall units $u^+ = \frac{u}{u_\tau}$ and $y^+ = \frac{y\, u_\tau}{\nu}$, as shown in figure 6. The greek letters ρ and ν represent the density and kinematic viscosity of the working fluid (water), respectively. It is interesting to note that the first experimental point is located just above the viscous sublayer, at approximately $y^+ = 5.9$, and the measured streamwise velocity, in wall units, at this point is $u^+ = 6.0$, remarkably close to the viscous sublayer theoretical law $u^+ = y^+$.

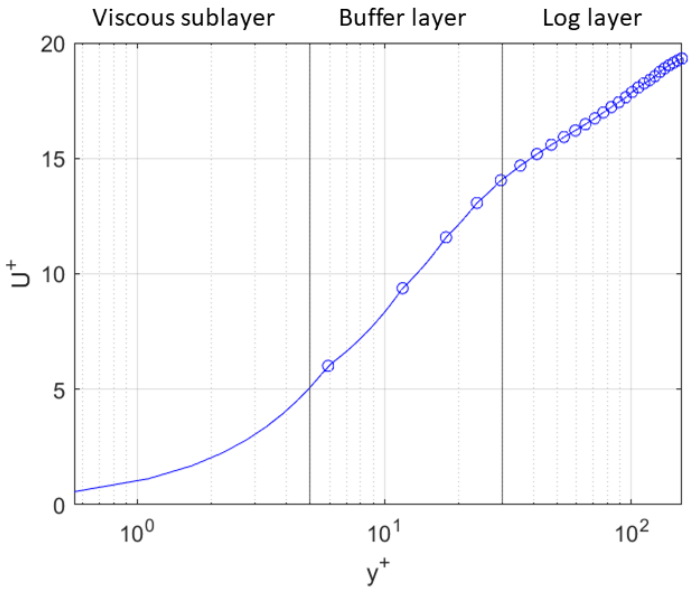

Figure 6 – Mean measured streamwise velocity profile in wall units. Reynolds number is 7000.

4.2 REYNOLS STRESS TENSOR MEASUREMENTS

Figures 7-12 present the comparison of all 6 components of the Reynolds stress tensor (second order statistics) from the Stereoscopic-PIV measurements performed, and the DNS data from Pinelli et al. (2010). Again, an excellent agreement can be observed.

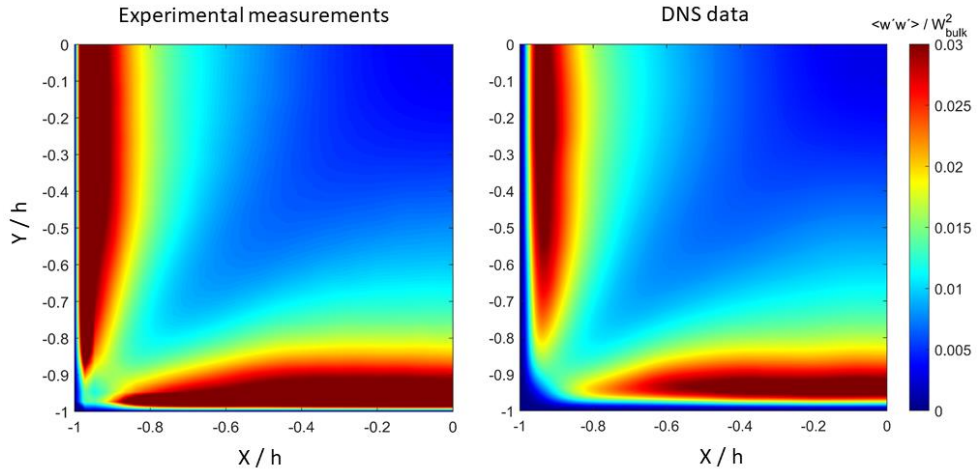

Figure 7 – Experimental and numerical comparison of the component < w´w´ > of the Reynolds stress tensor.

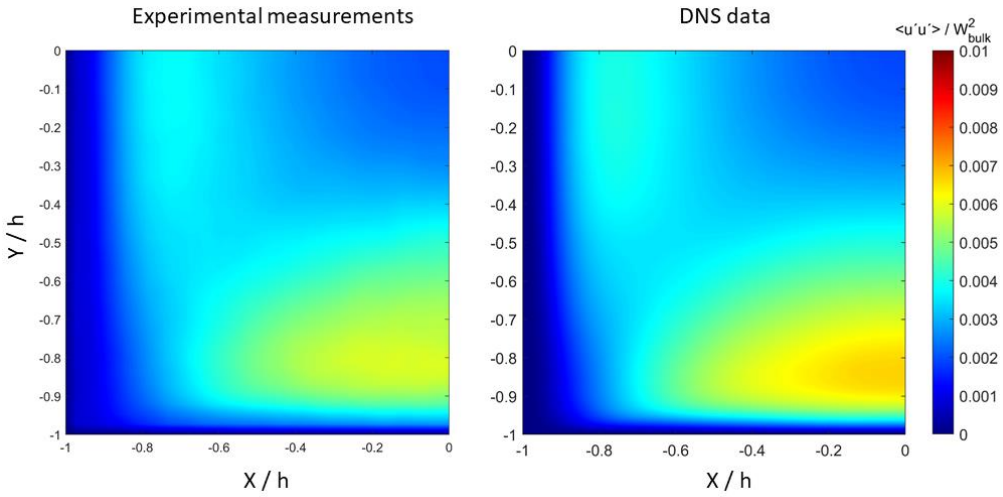

Figure 8 – Experimental and numerical comparison of the component < u´u´ > of the Reynolds stress tensor.

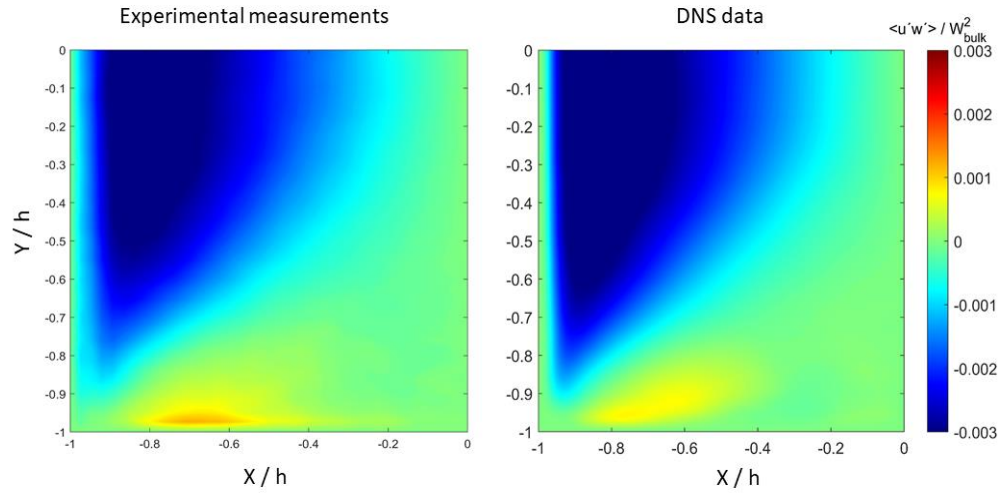

Figure 9 – Experimental and numerical comparison of the component < u´w´ > of the Reynolds stress tensor.

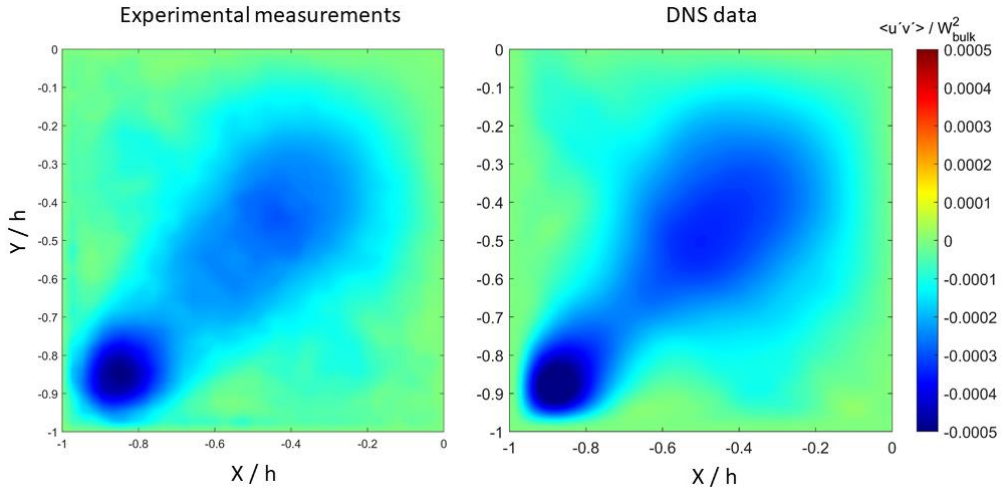

Figure 10 – Experimental and numerical comparison of the component < u´v´ > of the Reynolds stress tensor.

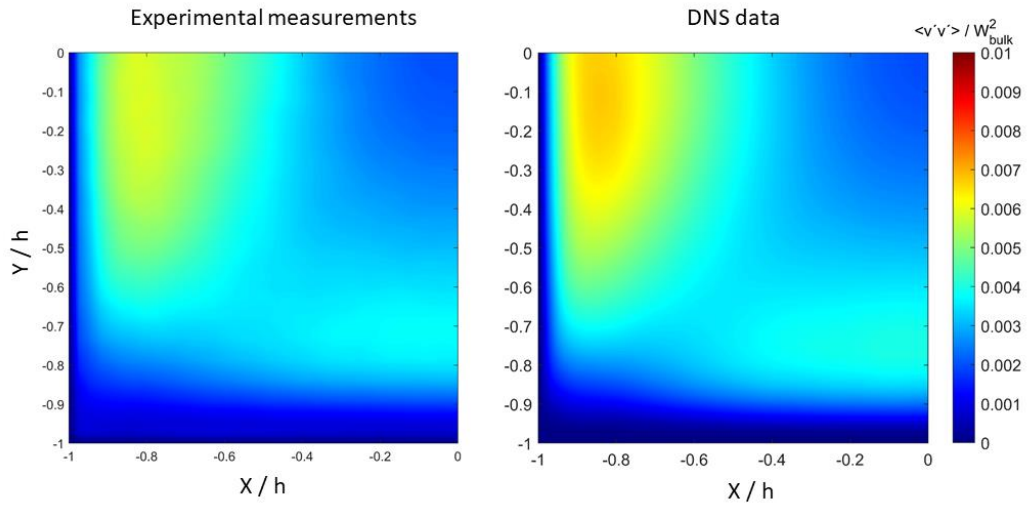

Figure 11 – Experimental and numerical comparison of the component < v´v´ > of the Reynolds stress tensor.

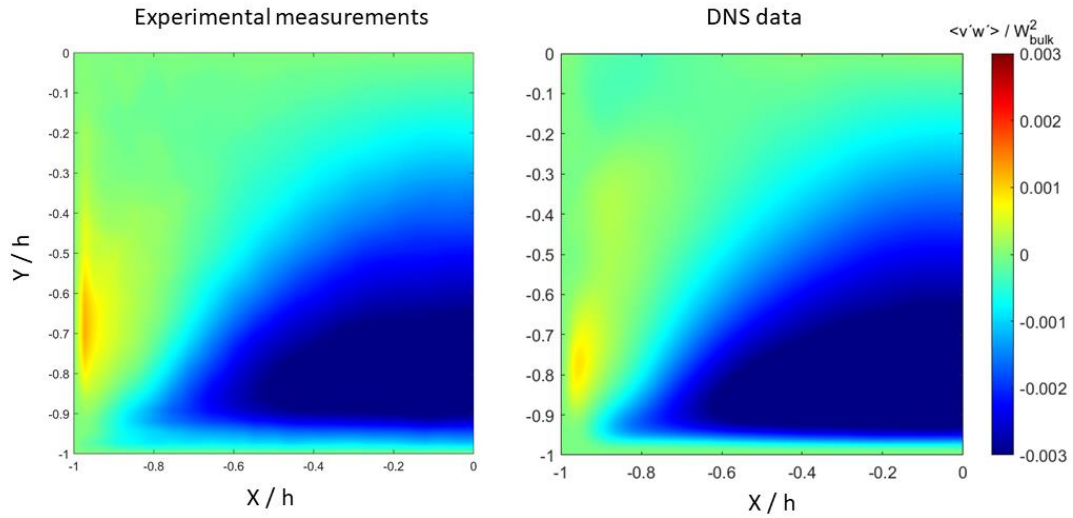

Figure 12 – Experimental and numerical comparison of the component < v´w´ > of the Reynolds stress tensor.

5. CONCLUSION

This work detailed part of an ongoing research effort being conducted at the Fluids Engineering Laboratory of PUC-Rio, with the aim of providing well-converged averaged velocity fields and Reynolds stress tensors information, in a square channel at high Reynolds number values. Preliminary results for the same Reynolds number of the Direct Numerical Simulations of Pinelli et al. (2010) at Reynolds number of 7000 were presented and compared, showing an excellent agreement and, therefore, validating the experimental procedure employed.

Data from Reynolds number ranging from 7000 to 42000 are currently being measured and processed. These data will be used both as a base case for the turbulent flow studies employing drag reducing agents (non-newtonian fluid) as well as to improve turbulence models via Machine Learning techniques. When performing data-driven turbulence modelling, one has to train a neural network or equivalent with high-fidelity data, which can be obtained either from a well-controlled experiment or from Direct Numerical Simulations. These steps are currently being developed in cooperation with researchers from COPPE/UFRJ.

6. ACKNOWLEDGEMENTS

The authors would like to acknowledge CAPES, CNPQ and Petrobras for the continuous financial support.

7. REFERENCES

Cruz, M.A., Thompson, R.L., Sampaio, L.E. and Bacchi, R.D., 2019. The use of the Reynolds force vector in a physics informed machine learning approach for predictive turbulence modeling. Computers & Fluids, 192, p.104258.

Gessner, F.B. and Jones, J.B., 1965. On some aspects of fully-developed turbulent flow in rectangular channels. Journal of Fluid Mechanics, 23(4), pp.689-713.

Gessner, F.B., 1973. The origin of secondary flow in turbulent flow along a corner. Journal of Fluid Mechanics, 58(1), pp.1-25.

Huser, A. and Biringen, S., 1993. Direct numerical simulation of turbulent flow in a square duct. Journal of Fluid Mechanics, 257, pp.65-95.

Launder, B.E., 1990. Phenomenological modelling: Present.... and future?. In Whither Turbulence? Turbulence at the Crossroads (pp. 439-485). Springer, Berlin, Heidelberg.

Moser, R., Kim, J., and Mansour, N. (1999). Direct numerical simulation of turbulent channel ow up to Reτ = 590. Physics ofFluids, 11(4):943-945.

K.A.M. Moinuddin, P.N. Joubert, M.S.Chong, Experimental investigation of turbulence-driven secondary motion over a streamwise external corner, J. Fluid Mech. 511 (2004), pp.1-23.

Pinelli, A., Uhlmann, M., Sekimoto, A. and Kawahara, G. Reynolds number dependence of mean flow structure in square duct turbulence. Journal of fluid mechanics (2010), 644, pp.107-122.

Spalart, P.R., 2000. Strategies for turbulence modelling and simulations. International Journal of Heat and Fluid Flow, 21(3), pp.252-263.

Uhlmann, M., Pinelli, A., Kawahara, G. and Sekimoto, A., 2007. Marginally turbulent flow in a square duct. Journal of fluid mechanics, 588, pp.153-162.

Vinuesa, R., Noorani, A., Lozano-Durán, A., Khoury, G.K.E., Schlatter, P., Fischer, P.F., Nagib, H.M., 2014. Aspect ratio effects in turbulent duct flows studied through direct numerical simulation. Journal of Turbulence, 15(10), pp.677-706.

8. RESPONSIBILITY NOTICE

The authors are the only responsible for the printed material included in this paper.